OCTOBER 14 2025

Measurement-based simulation of temperature rise from focused and linear ultrasound fields and its validation with experiments

Srinath Rajagopal ; Raphaela de Melo Baesso ; Piero Miloro ; Peter Harris; Ben Cox

J. Acoust. Soc. Am. 158, 2869–2882 (2025)
https://doi.org/10.1121/10.0039535

JASA ARTICLE

Measurement-based simulation of temperature rise from focused and linear ultrasound fields and its validation with experiments

Srinath Rajagopal,[1,a)] Raphaela de Melo Baesso,[1] Piero Miloro,[1] Peter Harris,[2] and Ben Cox[3]

[1]Ultrasound and Underwater Acoustics, National Physical Laboratory, Hampton Road, Teddington TW11 0LW, United Kingdom

[2]Data Analytics and Modelling, National Physical Laboratory, Hampton Road, Teddington TW11 0LW, United Kingdom

[3]Department of Medical Physics and Biomedical Engineering, University College London, Malet Place Engineering Building, Gower Street, London WC1E 6BT, United Kingdom

ABSTRACT:

Accurate quantification of acoustic fields produced by biomedical ultrasound devices is essential for assessing thermal and mechanical bioeffects on the patient. Device characterization involves time-consuming measurements, which need to be performed under many operating conditions for complete risk evaluation. Also, there are difficulties in measuring high-intensity therapeutic fields, which can damage the measuring devices. In this study, measurement-based simulations of temperature rise induced by ultrasound absorption in a tissue mimicking material (TMM) under linear propagation conditions were undertaken. The objective was to demonstrate a methodology for quantifying the accuracy of measurement-based simulations (a case study) along with an assessment of the uncertainties associated with both experimental and simulation setups. The acoustic and thermal modelling was performed using a pseudo-spectral time-domain solver, k-Wave. (Note that the methodology is not specific to this solver.) Ultrasound heating was conducted in the TMM with source acoustic power levels ranging from 1.1 to 4.3 W for durations of 2 to 4 min. The peak temperature rises recorded at the acoustic focus from the embedded fine wire thermocouples ranged from 4.4 (0.6) to 16.4 (1.3) °C. The difference in simulated temperature rises across all heating conditions with respect to measurements ranged from –1.9% to 6.7%.

 https://doi.org/10.1121/10.0039535

(Received 5 June 2025; revised 10 September 2025; accepted 15 September 2025; published online 14 October 2025)

[Editor: Charles C. Church] Pages: 2869–2882

I. INTRODUCTION

The ability to accurately quantify the acoustic field from biomedical ultrasound devices can facilitate improved prediction of thermal and mechanical bioeffects of ultrasound, such as local temperature rise or cavitation.[1–3] A complete characterization of transducer fields is time consuming to measure, in particular for multi-dimensional transducer arrays with complex geometry/transmit patterns. Furthermore, there are difficulties in measuring therapeutic ultrasound fields,[4,5] which can readily damage the measuring devices due to the effects of cavitation, mechanical stresses, and heat.[6–8] It is therefore necessary to use models for numerically predicting the acoustic fields.

In diagnostic ultrasound, the acoustic output quantities (acoustic pressure and intensity) are regulated through the use of safety parameters known as mechanical index (MI) and thermal index (TI).[9] These parameters provide the operator with a warning about the possible occurrence of cavitation effects and temperature rise, respectively, for a given scanner setting. Since *in situ* measurements are invasive and impractical, the acoustic field is quantified in water and then adjusted to allow for acoustic losses in equivalent path of tissue (acoustic derating),[10,11] which gives an estimate of *in situ* MI and TI. In therapy, safety is equally important in both ablative applications [e.g., high intensity therapeutic ultrasound (HITU) or histotripsy] and non-ablative applications (e.g., neuromodulation, opening of blood brain barrier and angiogenesis) where unsafe levels of ultrasound can permanently damage the underlying physiological functioning of the subjected anatomy.[4,12]

The measurement infrastructure for ultrasound field characterization includes hydrophones[13] to characterize the spatiotemporal field for pressures and intensities, radiation force balances (RFBs)[14–16] to determine the total acoustic output power from ultrasound transducers, and thermocouples (thin film and thin wire) to measure the surface temperature of externally applied transducer assemblies to assess hazards due to excessive heating of a patient.[9,17,18] The sensing devices are calibrated to ensure that the quantified parameters are traceable to the international system of units.[19,20] A recent review paper on pressure measurements in diagnostic and therapeutic ultrasound fields using hydrophones considered various issues such as their performance

[a)]Email: srinath.rajagopal@npl.co.uk

characteristics, calibration uncertainties, signal processing methods, and guidance on how to choose a hydrophone type for a given application.[21] Total ultrasound power is relatively straightforward to measure, and therapeutic ultrasound power levels, though challenging, can be measured with modified target configurations.[22,23]

It is possible to overcome the challenges of characterizing complex and high-intensity therapeutic fields by combining measurements with numerical simulation tools.[24–27] The method relies on using source conditions of the transducer, such as acoustic power measured using an RFB or source velocity distribution derived from measured near field two-dimensional (2D) hydrophone scans. The measured field parameters are then used together with transducer driving conditions and propagating medium properties in a chosen numerical wave solver to predict the acoustic field.

The study undertaken in this article demonstrates a methodology for quantifying the accuracy of measurement-based simulations (a case study) along with an assessment of the uncertainties associated with both experimental and simulation setups. The acoustic and thermal modelling was performed using a pseudospectral time-domain solver, k-Wave.[28–31] It is important to point out that the methodology is not constrained to any particular solver. The reference data for validation was obtained through an independent experiment. Fine wire thermocouples (TCs) were embedded in a TMM to record temperature rises caused by acoustic absorption from a focused ultrasound transducer. The electrical excitation conditions of the transducer ensured that the generated acoustic field in the TMM heating experiments was quasi-linear. The simulations were conducted under equivalent experimental conditions with the acoustic source in the simulation realized by reconstructing the source pressure distribution obtained from near field planar scanning of the focused transducer using a hydrophone. Therefore, the accuracy of the measurement-based simulation output is dependent on the experimental uncertainties of the simulation input parameters and the inherent uncertainties in the choice of the simulation tool—approximations in discretization of the governing equations, numerical scheme, and stability and convergence of the simulation grid.[32] It should be noted that there have been studies on qualitative[33–35] and quantitative experimental comparisons of k-Wave, such as wave propagation in skull phantoms[36] and nonlinear wave propagation in absorbing layered fluid media.[37] k-Wave has also been part of the intercomparison of fluid wave models against benchmarks set by the International Transcranial Ultrasonic Stimulation Safety and Standards (ITRUSST) consortium for transcranial ultrasound stimulation.[32] However, there have been fewer quantitative comparison studies of the heat diffusion model in the k-Wave toolkit.[38–40] Therefore, the quantitative comparison within this study was focused on evaluating uncertainty contributions in thermal measurements of experimental and numerical simulation setups.

The structure of the manuscript is as follows: The design of experiments is explained in Sec. II, and the development of the numerical model is presented in Sec. III. The uncertainty analysis is explained in Sec. IV, the results are presented in Sec. V and the discussion and summary are presented in Sec. VI. It is believed that the developed numerical model or the presented procedure could be used for predicting the thermal effects of ultrasound in various applications.

II. DESIGN OF EXPERIMENTS

In this section, the details of temperature rise experiments conducted in a cylindrical thermal test phantom made of agar based TMM are described. A focused ultrasound transducer (nominal diameter 64 mm and radius of curvature 63.2 mm) operating at a frequency of 1.06 MHz in continuous wave (CW) mode was used to induce temperature rise in the TMM and the temperatures were recorded using embedded thermocouples. Prior to temperature rise measurements, the transducer was calibrated using an RFB to produce four acoustic power levels in the range from 1.1 to 4.3 W. The driving voltages at the transducer input terminal were recorded to reproduce the acoustic powers for temperature rise measurements in the TMM immersed in a tank of water. Additional experimental details are provided in the supplementary material.

A. Thermal test phantom

The thermal test phantom (TTP) was designed to replicate the acoustic and thermal properties of soft tissues. It incorporated fine wire TCs with a diameter of 75 μm (model 5SRTC-TT-KI-40-1M, Omega Engineering, Manchester, UK), which is the smallest commercially available model with a mini-connector for data logger integration. Four TCs were distributed across the TTP body secured in a three-dimensional (3D) printed cylindrical holder with open ends. The height and the internal diameter of the cylinder were 58 and 70 mm, respectively. Grooves were cut into the cylindrical body to position the TCs at a depth of 20 mm from one end. The TCs external sheaths were removed, and the TCs were stretched such that the two wires were aligned in a plane perpendicular to the axis of the cylinder.[41] The junction of the thermocouple, TC0 was at the center of the cylinder and three other TCs (TC1, TC2 and TC3) were radially positioned at 2.5, 5, and 7.5 mm from the position of TC0. Agar based TMM was manufactured following the guidelines outlined in Annex DD.2 of the International Electrotechnical Commission (IEC) standard 60601-2–37.[9] The hot (56 °C) fluid form TMM was poured into the cylinder with one of its ends sealed using a polyethylene terephthalate (PET) film. The TMM solidified once it cooled down to room temperature, then the PET film was removed and that completed the TTP construction. A schematic of the TTP in the focus acoustic field of a focused transducer (model H101, Sonic Concepts, Bothell, WA USA) is shown in Fig. 1. The acoustic properties of the agar based TMM were assessed at the NPL (London, UK) material characterization facility,[42,43] while its thermal properties were

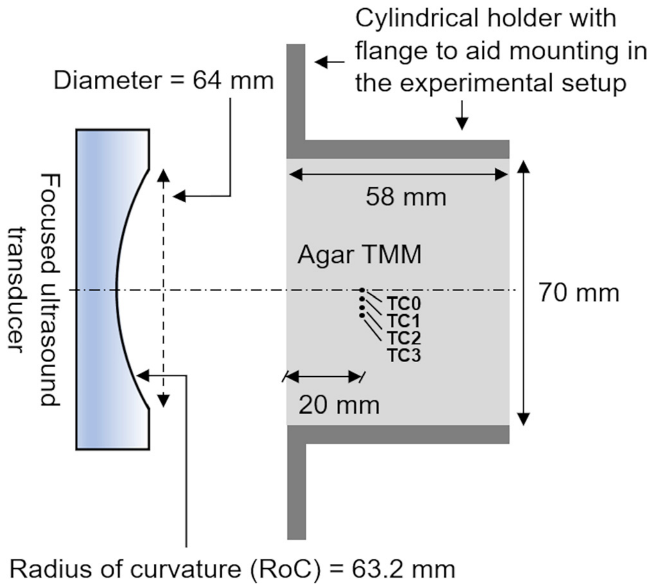

FIG. 1. A simple schematic of the thermal test phantom in the focused acoustic field of the focused transducer. Thermocouples TC0, TC1, TC2, and TC3 are embedded in an agar based TMM at a depth of 20 mm from the side facing the transducer. TC0 is at the center of the cylinder and three other thermocouples (TC1, TC2 and TC3) are radially positioned at a distance of 2.5, 5, and 7.5 mm from the position of TC0.

measured using a Tempos thermal property analyzer (SH-3 probe, Meter Environment, Pullman, WA). An independent assessment of the systematic uncertainty of the Tempos thermal property analyzer was not performed.

The physical properties of the TMM and water are listed in Table I. The values of water sound-speed and density at 19.1 °C were obtained using built-in k-Wave functions. The temperature and frequency dependent acoustic attenuation of water was calculated by fitting a 6th order polynomial fit to the measurement data given by Pinkerton.[44] Only a nominal uncertainty has been assumed for properties of water, whereas the uncertainties for TMM comes from a previous assessment.[42,43] The frequency dependent acoustic attenuation values of TMM measured at NPL (1–19 MHz) were fitted using MATLAB® with a power-law fit function of the form $\alpha_0 \times f^y$, where α_0 is acoustic attenuation coefficient [$\mathrm{dB \cdot cm^{-1}}$], f is frequency in MHz and y is the power-law exponent. The sound-speed dispersion of TMM can be obtained over the measured attenuation frequency range using the Kramers–Kronig relationship.[45] The stated accuracy for thermal properties is 10% based on Tempos manufacturer specifications. No further information was available regarding the statistical nature of the Tempos accuracy.

TABLE I. Physical properties of the TMM and water.

Physical property	Units	Value	Uncertainty
Density of TMM	$\mathrm{kg \cdot m^{-3}}$	1050	1% ($k=2$)
Density of water	$\mathrm{kg \cdot m^{-3}}$	998.4	0.1% ($k=2$)
Sound-speed of TMM	$\mathrm{m \cdot s^{-1}}$	1538 @ 1.06 MHz	0.33% ($k=2$)
Sound-speed of water	$\mathrm{m \cdot s^{-1}}$	1479.7	0.1% ($k=2$)
Attenuation of TMM	$\mathrm{dB \cdot cm^{-1}}$	$0.5519 \times f^{1.02}$	10% ($k=2$)
Attenuation of water	$\mathrm{dB \cdot cm^{-1}}$	$0.00217 \times f^2$	1% ($k=2$)
Thermal diffusivity of TMM	$\mathrm{mm^2 \cdot s^{-1}}$	0.16	10%
Volumetric heat capacity of TMM	$\mathrm{MJ \cdot m^{-3} \cdot K^{-1}}$	3.97	10%
Thermal conductivity of TMM	$\mathrm{W \cdot m^{-1} \cdot K^{-1}}$	0.62	10%

B. Measurement of acoustic power

The time-averaged acoustic power from the transducer was measured using an RFB technique.[16] The RFB technique is an established methodology used for measuring output power from planar, focused, and diagnostic ultrasound transducer probes.[14,15,23,46] The RFB setup at NPL is shown in Fig. 2. A total of four acoustic power levels (1.1, 2.2, 3.3, and 4.3 W) were measured by driving the transducer in CW mode, and their corresponding drive voltages were established. The linearity condition of the acoustic field at these power levels in the temperature rise measurements is discussed in the measurement uncertainty section (Sec. IV A 4).

C. Ultrasound heating setup

1. Multi-functional scanning system

The temperature rise measurements within the TTP were carried out using a multi-functional scanning tank (MFST) based on an ultrasound field scanning system (model UMS3, Precision Acoustics Ltd, Dorchester, UK). A representative schematic of MFST is shown in Fig. 3.

2. Alignment of the acoustic field within the thermal test phantom

The acoustic focus of the transducer was aligned along the propagation axis (z-axis) of the MFST via an iterative process.[47] The transducer was excited with 7.95 V_{rms}, 30-cycle tone burst and at a repetition rate of 200 Hz. A 0.2 mm active element diameter capsule type hydrophone (type HGL-0200, Onda Corporation, Sunnyvale, CA) was

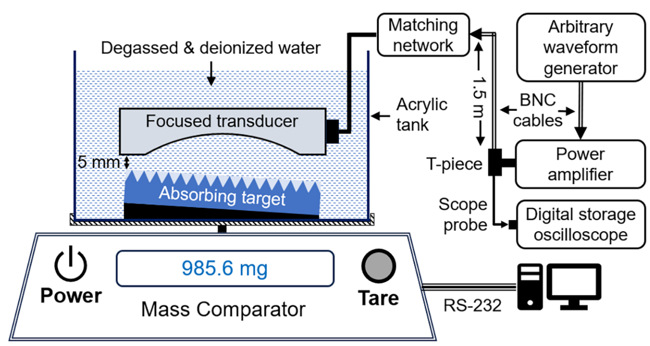

FIG. 2. RFB system in weigh-all configuration at NPL used to measure acoustic power. The dimensions of the water tank are 120 mm by 120 mm by 70 mm (length by width by height), which is filled with de-ionized and degassed water.

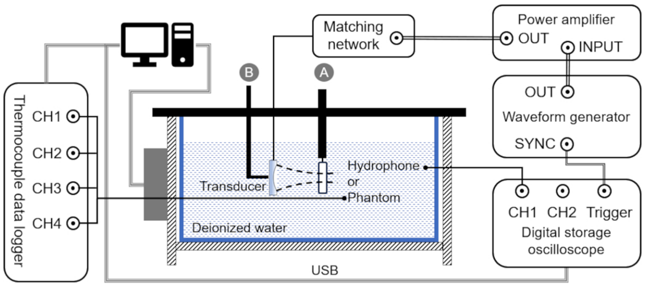

FIG. 3. A representative schematic of the multi-functional scanning tank (MFST) setup at NPL. A represents the computer controlled ultrasound field scanning system, and B represents a manual mounting fixture to hold transducers with five DOF with limited movement range in rotational and linear translation stages.

used to record the ultrasound signals. Once the acoustic axis was aligned, the hydrophone was replaced with the TTP, accounting for an additional 20 mm layer of agar based TMM in front of TCs. A TC data logger (model Pico USB TC 08, PicoTechnology, Cambridgeshire, UK) installed on Windows 10 computer was used to read the temperature of the four TCs. The transducer was driven at 1.06 MHz in CW mode at 11.1 V_{rms} equivalent to 2.2 W total acoustic power. A series of axial scans were performed independently across each axis (x, y, and z) with step sizes of 50 μm and settle time of 3 s between each step. The temperature rise of TC0 was monitored until the highest peak was identified. The system was considered aligned, indicating that the focal point was directly at the TC0.

3. Ultrasound heating measurements

The radiated acoustic powers measured on the RFB were reproduced in the heating measurement setup by driving the transducer at the previously established voltages. The TTP was exposed to heating durations of 2, 3, and 4 min from 1.1 W to 3.3 W and 2 min at 4.3 W. The temperature rise was monitored and logged at 1 Hz using the Pico USB TC 08 data logger. Each exposure was repeated three times, with a 20-min cooling period allowed between repetitions. For each repeat, a 60 s acquisition period was maintained before switching the transducer on to establish an appropriate baseline and to account for the exact time the system was activated. After the heating of TTP, the acquisition was continued for another 60 s.

III. NUMERICAL SIMULATIONS

The simulation tool used in this article was k-Wave, which is a third party MATLAB® (Matlab, Natick, MA) toolbox for time-domain numerical simulation of acoustic wave propagation and heat diffusion and perfusion based on the pseudospectral time domain method.[28–31]

The numerical simulations of the experimental setup are described in detail in the following subsection. First, an equivalent planar source of the focused bowl transducer was modelled from the near field raster scan using a hydrophone. Second, a 3D acoustic simulation was completed in water-TMM layered media with an equivalent source positioned in water. Third, the pressure field within the TMM layer was used to compute the heat source to simulate heating of the TMM. The temperature rise corresponding to the locations of four thermocouples in the thermal test phantom was recorded for comparison with measurements.

A. Equivalent source reconstruction of a focused transducer

A grid-based numerical approach was used for the acoustic model. For an accurate representation of the curved transducer in such a model,[48] the output of the transducer was measured over a plane perpendicular to the beam axis, and a planar equivalent source term was calculated.[49]

The specific measurement details related to the source reconstruction for the numerical model are briefly explained here. The hydrophone was a capsule type with an 85 μm active element diameter (HGL-0085, Onda Corporation, Sunnydale, CA) in combination with a 20 dB voltage gain preamplifier (AG-2020). The transducer was driven with a 30-cycle tone burst signal. The rms voltage of the drive signal at the input of the matching network of the transducer was 7.9 V_{rms}, which was equivalent to 1.1 W (Sec. V A). The acoustic focus of the transducer was aligned along the propagation axis (z-axis). A 2D planar scan was performed in the pre-focal region at a source-hydrophone separation of 30 μs time-of-flight (ToF) or 44.4 mm. The effective diameter of HGL-0085 at 1.06 MHz was determined by extrapolation using the effective diameters obtained from directional response measurements from 2 to 20 MHz.[50] A double exponential fit was applied to the measured data using MATLAB® and the resulting extrapolated value at 1.06 MHz was 532 μm. Also, the maximum effective hydrophone diameter calculated as per standard IEC 62127-1[51] for a given source geometry, frequency and measurement distance was 600 μm. Therefore, any errors due to spatial averaging were assumed to be negiligible.[51–53]

The hydrophone scan covered an area of 60 mm $\times$ 60 mm (201 $\times$ 201 grid points) at 0.3 mm step-size, which is $\sim$4.7 scan points-per-wavelength (PPW) that satisfied the 4.5 PPW criteria required for source reconstruction.[49] The hydrophone signal was sampled at 125 MHz on the oscilloscope, 12 500 sample points were recorded, and 256 waveform averages were performed at each scan position. The temperature of the water during the measurements in the scanning tank was 19.1 $\pm$ 0.5 °C.

Following the measurements, the hydrophone voltage waveforms at all scan positions were analyzed to calculate the pressure field. A stable voltage region after the first 20 cycles in the tone burst was identified, and an integer number of cycles (three periods) was extracted, and Fourier transformed to obtain the amplitudes and phases at the fundamental frequency of 1.06 MHz. The amplitude components were scaled using the voltage sensitivity of the hydrophone at 1.06 MHz to obtain the pressure amplitudes, and together with phases formed the complex 2D pressure field. This measured pressure field was used to compute the

JASA
https://doi.org/10.1121/10.0039535

equivalent planar source,[49] in a parallel plane immediately behind the curved surface. Since the reconstructed source would be larger than the scan area of the pre-focal region, the measured pressure field was expanded by zero-padding to a size of 512×512 grid points.

The pressure amplitude of the reconstructed complex source plane predicted using the numerical model with 30 iterations is shown in Fig. 4. The maximum absolute error, L_∞ and the root-mean-square (rms) error, L_2 in the modelled data relative to the measured data at the position of the measurement plane were 1.67% and 0.84%, respectively. These errors essentially describe the accuracy of the optimization process in reproducing the measured data from a 2D planar equivalent source compared to its physical counterpart, which has a curved surface. The accuracy of the reconstructed source is demonstrated by simulating the acoustic field in water and comparing it with axial and lateral beam profiles measured in water using a hydrophone (Sec. V A).

B. The acoustic simulation model

The 3D simulation for acoustic propagation consisted of water and TMM media in a side-by-side configuration that closely mimicked the measurement setup (see Fig. 5). The simulation grid was enclosed by a perfectly matched layer (PML), which is an unphysical acoustic anisotropic absorbing medium that completely absorbs the acoustic waves reaching the edges of the computational domain. The PML size was set to 20 grid points in x, y, and z dimensions. The source plane was positioned in a water medium that was offset by five grid points away from the PML boundary. The thickness of the water region from the source plane to water-TMM interface was 42.76 mm and the thickness of the TMM region was 20 mm, which matched the measurement setup. As seen in Fig. 4, there are large noncontributing regions outside of the circular source area, which were excluded and reduced to a size of $97.2 \times 97.2\,\text{mm}^2$. The 3D grid dimensions, including the PML were $97.2 \times 97.2 \times 97.2\,\text{mm}^3$.

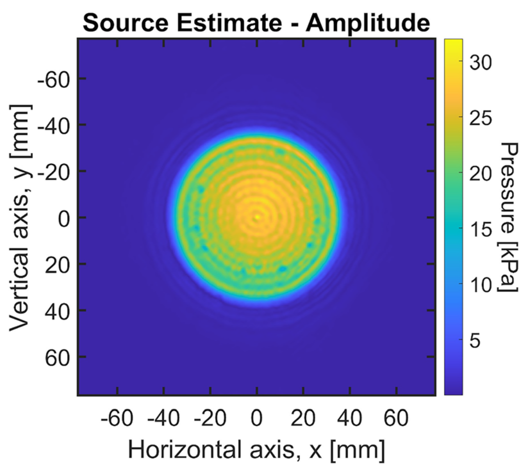

FIG. 4. The pressure amplitude map of the reconstructed complex source plane predicted using the numerical model with 30 iterations. The L_∞ and L_2 errors at the 30th iteration were 1.67% and 0.84%, respectively.

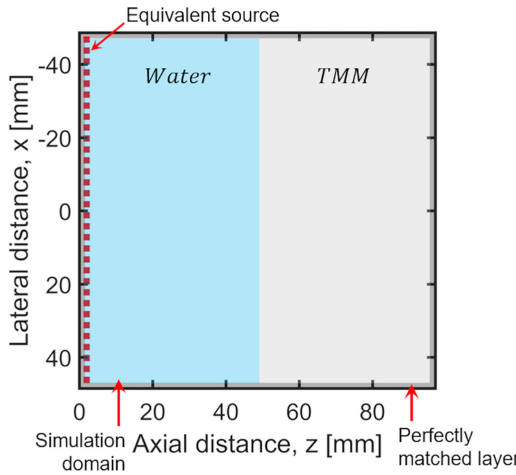

FIG. 5. Schematic of the 3D simulation grid represented in 2D. A PML composed of 20 grid points encloses the simulation domain where the acoustic equations are solved. The red squares represent the equivalent source obtained in Sec. III A, which is offset by five grid points from the PML. The thickness of the water layer is ∼42.76 mm matching the experimental setup, whereas the thickness of the TMM (∼51 mm) is sufficient to contain pre- and post-focus acoustic field.

The medium properties used in the simulation are listed in Table I. The simulation was run with a single frequency CW source for a duration of 120 μs, which is slightly longer than duration required for an acoustic wave to travel across the diagonal axis. The amplitudes and phases of the source were used to calculate the time varying sinusoidal source signals. The steady state pressure field was estimated by calculating the amplitudes of the acoustic waves from two integer cycles of each time series at the end of the simulation across the entire simulation grid. The pressure field obtained at 1.1 W was scaled to produce fields corresponding to 2.2, 3.3, and 4.3 W acoustic powers by using the respective drive voltages relative to voltage at 1.1 W.

C. Convergence testing of the acoustic simulation model

The stability and accuracy of the acoustic simulation is governed by the Courant-Friedrichs-Lewy (CFL) number $\text{CFL} \equiv c_0 \Delta t / \Delta x$. Here, c_0 $[\text{m} \cdot \text{s}^{-1}]$ is the medium sound-speed, Δt [s] is the simulation time step, and Δx [m] is the spacing between grid points. When the medium is heterogenous, c_0 in CFL is replaced by the maximum value of the sound-speed, c_{max} in the medium. A CFL value of 0.3 is usually sufficient for weakly heterogenous media, however, for strongly heterogenous media, a much smaller CFL would be necessary to ensure grid stability. In the present case, though the sound-speeds and densities are comparable to within a few percents, the acoustic attenuation of TMM is two orders of magnitude higher than that of water. Consequently, sufficiently small values of Δx and Δt are needed to ensure the acoustic simulation is stable and accurate. The acoustic simulations were run by successively decreasing the values of Δx and Δt until the output from the simulations did not change significantly. Note that the size of PML was kept at 20 grid points during convergence testing.

Three spatial grid steps of 300, 150, and 75 μm were considered. The input source planes for 150 and 75 μm grid steps were estimated by resampling the reconstructed complex source plane at 300 μm grid step using the Fourier interpolation. For each of Δx, three simulations were run using time steps of 60.8, 15.2, and 3.8 ns. The maximum pressure amplitude from each of the simulation was compared to examine convergence (see Table II). The time step, Δt was controlled by successively halving the CFL value from an initial value of 0.3. For each spatial grid step, the corresponding number of grid points-per-wavelength, PPW, is also included in Table II. It can be seen from Table II that when Δx is 75 μm or 18.8 PPW, the change in pressure amplitude for the two values of Δt of 15.2 and 3.8 ns is negligible, indicating the convergence of the acoustic simulation model. Overall, the pressure amplitudes in Table II are not significantly different, and the maximum change in pressure amplitude relative to the smallest pressure amplitude is only 4.2%. However, since intensity is proportional to pressure squared, the error in temperature rise predictions would be 8.8%, i.e., twice the error in pressure convergent value. Therefore, this would drastically impact the quantitative comparison between measurement and model, which is the main purpose of the present study. Therefore, the steady state pressure field obtained from the convergence test for $\Delta x = 75$ μm and $\Delta t = 3.8$ ns was used in thermal simulations. Uncertainty arising from the chosen grid is considered in Sec. IV B 2.

D. Temperature rise in the TMM

In this final step, only the pressure distribution within the TMM region is required for temperature rise predictions. Therefore, the pressure inside the TMM region ($43.2 \times 43.2 \times 43.2\,\text{mm}^3$) was used in the subsequent steps. The heat diffusion equation was solved using a pseudo-spectral model (k-Wave) in which the heat source term is the volume rate of heat deposition, Q [$\text{W} \cdot \text{m}^{-3}$], due to ultrasound absorption, defined as $Q = \alpha(f)p^2/c_0\rho_0$, where $\alpha(f)$ is the frequency dependent acoustic attenuation of TMM in units of Neper $\cdot\, \text{m}^{-1}$, p [Pa] is the amplitude of the steady state pressure field distribution inside the TMM, c_0 [$\text{m} \cdot \text{s}^{-1}$] is the sound-speed and ρ_0 [$\text{kg} \cdot \text{m}^{-3}$] is the density of TMM. The medium properties of the TMM are already listed in Table I. The initial temperature distribution within the TMM was assumed same as the water bath in the experiments. The heat source duration was set to be the same as the heating times in the experiments (i.e., 2, 3, or 4 min). The thermal simulation was continued for 1 min after the heat source (ultrasound) was turned off. The time step was set to 1 s, as in the experiments. The temperature time-series were recorded at the position of maximum acoustic pressure across all grid points on the horizontal axis to the direction of acoustic wave propagation. The temperature data on the grid points corresponding to the measurement locations were used for quantitative comparison.

TABLE II. Maximum acoustic pressure amplitude recorded from the convergence test for each value of spatial grid step, Δx and time step, Δt. PPW is the corresponding number of grid points-per-wavelength.

		Δt		
Δx	PPW	60.8 ns	15.2 ns	3.8 ns
300 μm	4.7	849.6 kPa	841.5 kPa	840.1 kPa
150 μm	9.4	867.5 kPa	863.1 kPa	862.6 kPa
75 μm	18.8	878.1 kPa	876.8 kPa	876.7 kPa

IV. MEASUREMENT AND SIMULATION UNCERTAINTIES

In this section, the uncertainty components of the measurement setup (Sec. IV A) and numerical simulation (Sec. IV B) are identified, and the approaches to quantify those components are described. The summarized uncertainty components combined to give an expanded uncertainty for a specified coverage probability of 95% are presented (Sec. IV C). The uncertainty assessment presented in this study is consistent with the "Guide to the expression of uncertainty in measurement (GUM)" document series published by the Joint Committee for Guides in Metrology.[54]

A. Uncertainty contributions arising from the measurements

1. Viscous heating effect of the thermocouple

The size of the TC is critical to minimizing ultrasound-induced temperature rise, i.e., viscous heating artefacts,[55,56] which can lead to a significant overestimation depending on the size and type of TC.[57,58] Additionally, sources of error arise from the thermal conductivity and differences in heat capacity and density between the TC wire and the surrounding tissue during ultrasound heating. In the present study, the diameter of the TC was $1/19$ of the ultrasound wavelength and the resulting errors arising from the chosen TC size were quantified.[56] Reference 59 reported a comprehensive comparison of five correction methods[55,60,61] to account for viscous heating artifacts on measurements made using a 75 μm diameter TC embedded in a TMM for acoustic powers ranging from 20 to 50 W. There was a large variation between the methods, for example, at 20 W the standard deviation was 23% and the mean difference with respect to measurement was –28%. A standardized method for correcting viscous heating artefacts is difficult since a number of experimental conditions influence the results, such as the type of ultrasound excitation (CW or pulsed),[58] increased risk of cavitation,[60] type, and even aging of thermocouple.[57]

For the present study "wait then measure" correction method was applied.[55] In this method, the rapid rate of change of temperature due to viscous heating, which occurs at the moment of transducer switch-on, is compensated by delaying the measurement by a fixed amount of time. In practice, the correction is applied by subtracting the temperature read by the TC at 0.5 s after the switch-on transition across the temperature-time recording.[55] Since the temperature readings were acquired at 1 s interval, the data were interpolated using the nearest neighbor method to obtain the correction value at 0.5 s. Given the wide variation reported in Ref. 59, an additional uncertainty expressed as the semi-width of a rectangular distribution was included, which was calculated as a fraction of the correction value to the uncorrected peak temperature.

2. Accuracy of the thermocouple

It was important to assess the accuracy of the TCs used in this study since the temperatures measured in the TTP served as a reference for comparison with simulated values. As per manufacturer's specifications, the resolution of the data logger with K-type TC is 0.025 °C, over a range of –250 °C to 1370 °C, which is small and hence no uncertainty contribution was included. Ideally, an *in situ* calibration of the TCs is needed for which no method currently exists. Therefore, the calibration data of two TCs identical to those used in the TTP, each calibrated along with a PicoLog 6 data logger, were examined. The calibration was performed from 20 °C to 50 °C in steps of 5 °C in terms of the International Temperature Scale of 1990. The expanded uncertainty ($k = 2$) of calibration was 0.02 °C. For both probes, a negative correction was specified, which depended approximately linearly on temperature from −0.38 °C to −0.22 °C and −0.15 °C to −0.4 °C. No corrections were applied to the temperature-time recordings since the slopes of the TC correction were of opposite sign. Considering the non-availability of performance data for TCs embedded in materials such as TTP, a worst-case uncertainty of 10% expressed as the semi-width of a rectangular distribution was included for the lowest peak temperature and proportionally lower uncertainties were included for higher peak temperatures.

3. Acoustic power

The RFB setup described in Sec. II B is the NPL's secondary standard traceable to a primary standard RFB, which has been subjected to international intercomparison with similar institutions following an agreed protocol of measurements.[19] The overall measurement uncertainty encompasses a number of systematic components such as balance resolution and its linearity, extrapolation to the moment of switching the transducer on/off to determine the change in mass, absorbing target imperfections, the diameter of the transducer relative to target diameter, temperature of water, plane wave assumptions, acoustic absorption in the water path between the transducer and target, accuracy in the measurement of transducer drive voltage and random variation from a set of repeat measurements.[14] The combined expanded uncertainty ($k = 2$) in the measurement of all four powers was 4%. The peak temperatures for ultrasound heating durations of 2, 3, and 4 min were found to be a linear a function of acoustic power with coefficients of determination, R^2 better than 0.99.

4. Acoustic nonlinear propagation

The acoustic nonlinearity parameter, B/A, for water and TMM are similar.[51,62] The acoustic attenuation at 20 °C for water and TMM at 1.06 MHz are 0.0025 and 0.6 $\text{dB} \cdot \text{cm}^{-1}$, respectively, which is more than two orders of magnitude higher for TMM relative to water. Therefore, any acoustic nonlinearity in the focal region of TMM should be negligible. A test was performed in water by placing an HGL-0085 calibrated hydrophone at the focus, and a tone burst waveform was acquired by driving the transducer at a previously determined acoustic power of 4.3 W. The first harmonic pressure amplitude was 1.9 MPa, and the second harmonic level was lower by 26.3 dB. Furthermore, the unitless local distortion parameter,[63] σ_q was estimated, but with two deviations. Since the lateral acoustic pressure profiles were approximately symmetric (see Fig. 6), the beam area was calculated from the average radius of pulse-pressure squared integral profiles in the x and y axes at 4.3 W driving condition. The source aperture area was calculated using the geometrical diameter of the transducer. The estimated σ_q was 0.02, which is much lower than the threshold value of 0.5, indicating a little distortion has occurred.[63] Therefore, only a small uncertainty contribution of 1% expressed as the semi-width of a rectangular distribution was included.

5. Repeatability of the ultrasound heating setup

The TTP measurements were repeated independently three times using the ultrasound heating setup described in Sec. II C. For each repeat measurement, the TTP was removed from the MFST, remounted, and realigned in the focused acoustic field before recording the temperature profiles at nominal acoustic power levels of 1.1, 2.2, 3.3, and 4.3 W. The standard errors estimated from the standard deviations of three repeat measurements for each heating condition were included in the uncertainty budget. Across all measurements for thermocouple TC0, the standard error was found to be less than 1%, which suggested that the ultrasound heating setup was stable, and the measurement protocol described in Sec. II C was acceptable and repeatable.

B. Uncertainty arising from the numerical model

1. Equivalent source reconstruction

The process of equivalent source reconstruction incurs errors from three contributions: (i) The source reconstruction is an optimization algorithm and therefore, even with numerically generated measurement data (noise free), the L2 error was previously shown to converge within 0.2%.[49] Therefore, the L_2 error of 0.84% from the present study, which is expressed as the semi-width of a rectangular distribution, was included in the uncertainty budget. (ii) Accuracy of mapping the 2D pressure field. This contribution is influenced by consistent operation of the MFST in stepping the hydrophone during raster scan without loss of position increment or accumulation of stepping errors, how well the hydrophone was aligned to the acoustic propagation

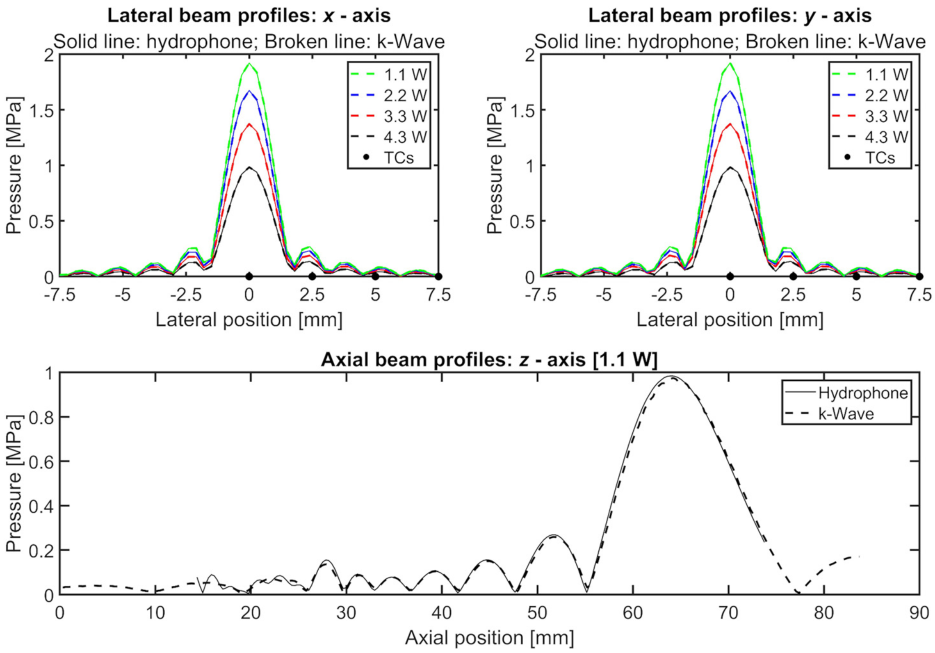

FIG. 6. Axial and lateral beam profiles from hydrophone measurements (solid line) and k-Wave acosutic simulations (broken line) in water-only medium. For indication, the solid black dots represent the position of TCs in the TTP with respect to the structure of acosutic field.

axis, extent of the 2D pressure field captured, stability of the transducer drive system, signal-to-noise ratio of the hydrophone and the temperature stability of the water in the tank. The quality of the measured data increases the likelihood of convergence to a lower error value, or else the optimization may not converge at all. It was difficult to independently evaluate the effect of each component of the field mapping process on the source reconstruction. However, judging by the repeatability observed in the ultrasound heating measurements, a conservative estimate of 2% was expressed as the semi-width of a rectangular distribution was included. (iii) The hydrophone may be considered independent of the reconstruction algorithm since the optimization process is not dependent on the hydrophone calibration accuracy. The algorithm is concerned with reproducing the measured data produced by a curved source to its planar equivalent. However, hydrophone calibration accuracy is important to ensure that the acoustic powers realized via acoustic simulations (Sec. III B) are approximately the same powers measured on the RFB for identical transducer excitation conditions. Therefore, uncertainty in the magnitude calibration of the hydrophone used to map the 2D pressure field (6% at $k = 2$) is considered within the equivalent source reconstruction.

2. Acoustic model convergence

The results of the acoustic model convergence test are presented in Table II. The time step Δt was controlled by the CFL number, so halving CFL decreased the value of Δt by a factor of 4. Consequently, the acoustic model converged faster with decreasing Δt than grid step, Δx, which was decreased by a factor of 2. For a Δx of 75 μm, the variation in pressure values with Δt can be considered negligible, whereas for a Δt of 3.8 ns, the change in pressure with Δx from 300 μm to 150 μm and 150 μm to 75 μm was 2.7% and 1.6%, respectively. If the computing resources were available to test a lower grid-spacing, Δx of 37.5 μm, then the acoustic model would be within 1% of the convergent value. An uncertainty of 1% expressed as the semi-width of a rectangular distribution was included in the uncertainty budget.

3. Simulation input parameters

The acoustic and thermal simulations include several measured input parameters, which are subject to a degree of uncertainty as discussed in Sec. IV A. Therefore, a Monte Carlo (MC)[64] method was used to assess the contribution from these parameters by perturbing the simulation input parameter values and repeating the simulations. It should be noted that acoustic simulations were not subject to MC method since it was computationally burdensome. For example, the largest acoustic simulation ($\Delta x = 300\,\mu$m and $\Delta t = 3.8$ ns) took 70.2 h to obtain the acoustic pressure distribution in the water-TMM media. Each heating condition of the thermal simulations took less than 30 min for completion. Therefore, for practical reasons only thermal simulations were feasible for MC method.

For the thermal simulations, acoustics and thermal properties of TMM are required, which are listed in Table I along with their estimated uncertainty and coverage interval (k) where available. The TMM input parameters were drawn randomly from either a normal or uniform distribution with standard deviations equal to their standard uncertainties. For example, sound-speed of TMM was perturbed using the MATLAB® function "`normrnd(1538, 5/2)`," where divisor 2 is the k value. The accuracy of 10% in the measured thermal properties of TMM was assigned a rectangular distribution in the absence of further statistical information from the Tempos manufacturer. Therefore, their standard uncertainties were derived after dividing the accuracy by $\sqrt{3}$. The relevant MATLAB® function was "`unifrnd`." A total of 1000 simulations were performed, and for each simulation, all input parameters were perturbed together. The histogram plots of peak temperatures for all heating conditions showed that the temperatures from 1000 simulations were normally distributed. Consequently, a standard uncertainty equal to the standard deviation calculated from 1000 simulations for each heating condition was included in the uncertainty assessment.

C. Uncertainty tables

The uncertainty components of the experimental setup and numerical simulations are determined in Secs. IV A and IV B are listed in Tables III and IV. The uncertainties in Table III are tabulated for three driving conditions of the transducer: 1.1 W for 2 min, 2.2 W for 3 min, and 4.3 W for 2 min. The resulting peak temperature rises measured at TC0 were 4.4 °C, 9.6 °C, and 16.4 °C. Since the relative placement errors for thermocouples TC1, TC2, and TC3 could not be ascertained with confidence in the physical TTP no uncertainty contribution was included. Therefore, Table III is primarily concerned with the accuracy of temperature rise measurements from TC0. Since the acoustic focus was aligned to the response of TC0 (Sec. II C 2) and three independent repeat measurements were undertaken, standard error evaluated from standard deviations of repeat measurements were deemed sufficient.

In Table IV, uncertainties in the simulations are tabulated for three driving conditions of the transducer: 1.1 W for 2 min, 2.2 W for 3 min, and 4.3 W for 2 min. The resulting peak temperature rises obtained from the simulations at the acoustic focus were 4.6 °C, 9.7 °C, and 17.5 °C, which corresponded to the location of TC0 in experiments. Note that the uncertainty components have been doubled except for the thermal model input parameters since intensity is proportional to the square of the pressure amplitude, which was used in the calculation of the heating source in thermal simulations.

V. RESULTS

A. Equivalent source simulations in water and its comparison with hydrophone measurements

The results of the acoustic simulation in water-only medium using the equivalent source and its comparison with the hydrophone measurements are shown in Fig. 6. The grid structure was similar to water-TMM setup (Fig. 5) except that TMM was replaced by water and Δx and Δt were 300 μm and 58.9 ns (CFL = 0.3), respectively. The hydrophone was axially aligned, and an axial profile was measured at 1.1 W. At the focal maximum pressure, lateral beam profiles were measured for all four power levels. The hydrophone scan step size in axial and lateral directions was kept constant at 300 μm. The maximum relative mean square error across all the simulated lateral beam profiles against hydrophone measurements was 0.8%, which is similar the L2 error in Sec. III A.

B. Measured transducer acoustic output powers and focal intensities

The radiated acoustic output powers from the transducer, measured using the RFB along with the corresponding drive voltages and focal intensities, are listed in Table V. The measured lateral beam profiles (Fig. 5) were fit with a Gaussian curve to obtain the −6 dB beam width, which was 1.8 mm and the consequent −6 dB beam area was 2.54 mm^2 (0.025 cm^2). The beam area measured in water was assumed to be similar in TTP. The measured radiated output was attenuated using the relation $P_z = P_0 \exp(-2\alpha z)$, where P_0 is the radiated power, P_z is the attenuated power along the beam axis at a distance z, and α is the amplitude attenuation coefficient of plane acoustic waves in a given medium. The P_0 was attenuated using two values of α for water and TMM over a distance of 42.76 mm and 20 mm, respectively.

The uncertainties listed alongside the values for the drive voltage and power are expanded uncertainties stated at a coverage probability of 95% ($k = 2$). The expanded uncertainties in intensities were estimated by combining the uncertainties in power, beam width, and acoustic amplitude attenuation coefficient of TMM.

C. Example of temperature distribution in TMM from simulations

An example temperature distribution within the TMM from thermal simulations is shown in Fig. 7 for the case of 4 W applied power and 2-min heating duration. The left panel in Fig. 7 was the temperature distribution at the end of

TABLE III. A representative uncertainty budget for the experimental setup used to measure temperature rise in TTP. The combined expanded uncertainty is stated at a coverage probability of approximately 95% ($k = 2$). UC, uncertainty; Std. UC, standard uncertainty.

			1 W; 2 mins		2 W; 3 mins		4 W; 2 mins	
Source of uncertainty	Probability distribution	Divisor	UC [%]	Std. UC [%]	UC [%]	Std. UC [%]	UC [%]	Std. UC [%]
Viscous heating effect	Rectangular	$\sqrt{3}$	4.80	2.77	3.10	1.79	3.10	1.79
Thermocouple accuracy	Rectangular	$\sqrt{3}$	10.0	5.77	8.40	4.85	5.00	2.89
Acoustic power	Normal	2	4.00	2.00	4.00	2.00	4.00	2.00
Acoustic nonlinearity	Rectangular	$\sqrt{3}$	1.00	0.58	1.00	0.58	1.00	0.58
Standard error ($n = 3$)	Normal	1	0.23	0.23	0.29	0.29	0.02	0.02
Combined Std. UC /%	Normal	—	—	6.7	—	5.6	—	4.0
Expanded UC /%	Normal ($k = 2$)	—	—	13.5	—	11.2	—	8.0

TABLE IV. A representative uncertainty budget for the numerical simulations implemented using k-Wave to simulate the temperature rise in TMM. The combined expanded uncertainty is stated at a coverage probability of approximately 95% ($k = 2$). UC, uncertainty; Std. UC, standard uncertainty; Std. Dev, standard deviation.

			1 W; 2 mins		2 W; 3 mins		4 W; 2 mins	
Source of uncertainty	Probability distribution	Divisor	UC [%]	Std. UC [%]	UC [%]	Std. UC [%]	UC [%]	Std. UC [%]
Hydrophone calibration	Normal	2	12.0	6.00	12.0	6.00	12.0	6.00
Hydrophone scanning system	Rectangular	$\sqrt{3}$	4.00	2.31	4.00	2.31	4.00	2.31
Equivalent source, L2 error	Rectangular	$\sqrt{3}$	1.68	0.97	1.68	0.97	1.68	0.97
Acoustic model convergence	Rectangular	$\sqrt{3}$	2.00	1.15	2.00	1.15	2.00	1.15
Std. Dev in MC simulations of thermal model	Normal	1	8.70	8.70	9.10	9.10	8.90	8.90
Combined Std. UC	Normal	—	—	10.9	—	11.2	—	11.1
Expanded UC	Normal ($k = 2$)	—	—	21.9	—	22.5	—	22.2

the heating duration, and on the right panel, it was the temperature distribution 60 s after the transducer was switched off. The white dots represent virtual TC positions spaced 2.5 mm apart on the computational grid. The temperature-time data at these grid positions were recorded for comparison with TCs embedded in TTP (see Fig. 8).

D. Examples of temperature-time data from measurement and simulation

Temperature-time plots obtained from the measurements (dashed lines), which were not corrected for viscous heating effects, and simulations (solid lines) are presented in Fig. 6. It should be noted that the background temperature (19.1 °C) in the measurements and simulations was removed to aid better comparison. The plots represent the data from four heating conditions: 1.1 W for 2 min, 2.2 W for 3 min, 3.3 W for 3 min, and 4.3 W for 2 min. The measured and predicted temperatures are very similar for all TCs, except TC1. The measured temperatures of TC1 are higher than the predicted results for all four cases. In a simulation study, the viscous heating effect was also seen in the sidelobes of focused field; however, its effect was lower compared to the TC placed at focus.[57] Therefore, it is unlikely that the cause of higher TC1 recordings was due to increased heating from side lobes. The closest simulation grid point that gave a close agreement with measurement at TC1 was 1.8 mm from TC0, a difference of 0.7 mm. Therefore, it is likely that that TC1 may have been placed closer to TC0 during TTP fabrication.

TABLE V. Transducer drive voltages measured at its input terminal and the corresponding radiated acoustic output powers realized on the RFB. Focal intensities are approximated as described in Sec. V A. The parenthetical values are expanded uncertainties stated at a coverage probability of approximately 95% ($k = 2$).

Voltage [V_{RMS}]	Radiated power [W]	Focal intensity [$W \cdot cm^{-2}$]
7.90 (2%)	1.1 (4%)	33 (18%)
11.1 (2%)	2.2 (4%)	65 (18%)
13.6 (2%)	3.3 (4%)	98 (18%)
15.5 (2%)	4.3 (4%)	128 (18%)

E. Viscous heating corrections

The viscous heating corrections (VHCs) obtained using the "wait then measure" method are listed in Table VI. Each correction value represents an average from three repeat

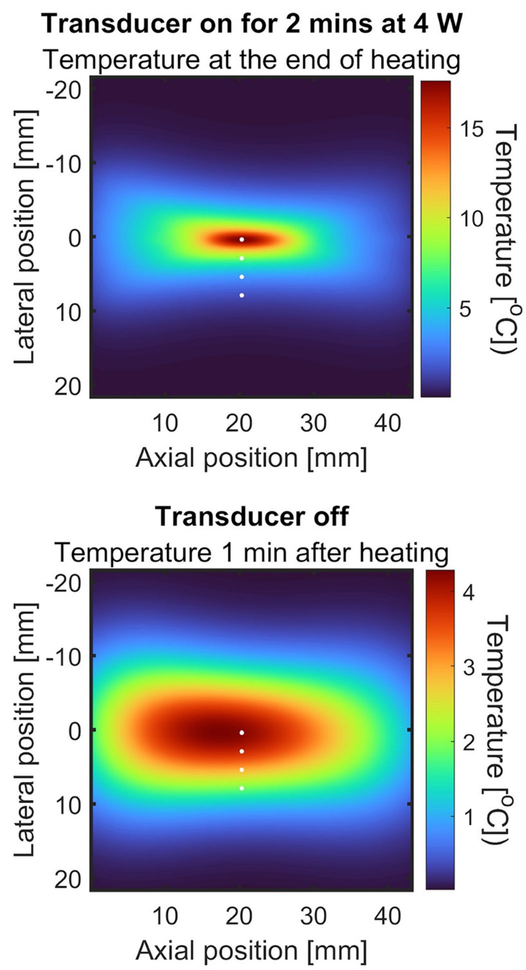

FIG. 7. Temperature distribution within the TMM from thermal simulations for the case of 4.3 W applied power and 2-min heating duration. Top panel, temperature map at the end of heating. Bottom panel, temperature map after the transducer was switched off for 1 min. The white dots represent the TC positions spaced 2.5 mm apart from the position of maximum temperature grid point.

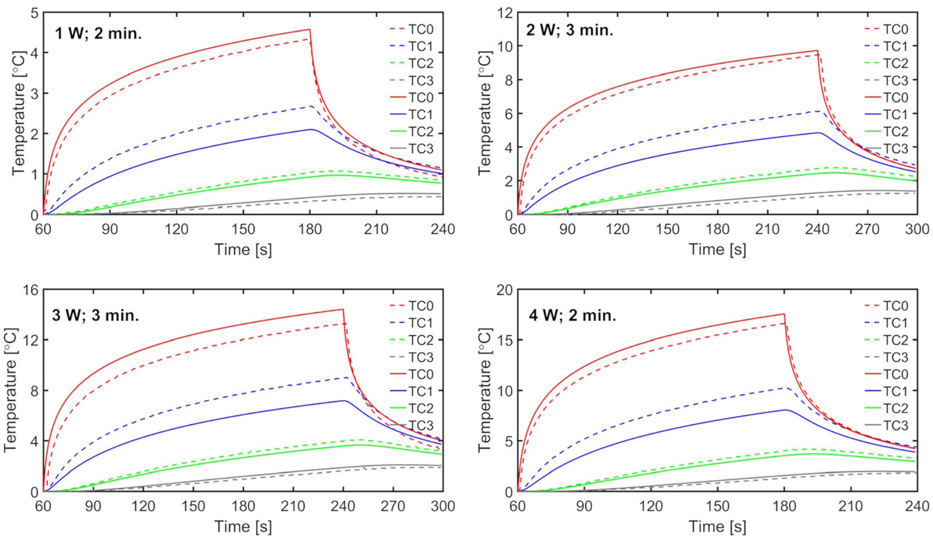

FIG. 8. Temperature-time plots for various powers from simulations (solid lines) and measurements (dashed lines), which were corrected for viscous heating effects using "wait then measure" method. The background temperature (19.1 °C) in the measurements and simulations was removed to aid better comparison.

heating measurements. For the uncertainty, the standard deviation in the uncorrected and corrected peak temperatures for the three repeat measurements was calculated and added together in quadrature. There appears to be some dependence of VHC on intensity. In a previous study,[24] which used a 50 μm diameter fine wire TC embedded in a hydrogel-based TMM, the VHC corrections were obtained by fitting a best fit (cubic) curve to the TC data. A data window from 2 to 12 s after the peak temperature was used for curve fitting and using the best fit coefficients, the temperature to the time at peak temperature was extrapolated. Their VHCs at 24 $W \cdot cm^{-2}$ and 102 $W \cdot cm^{-2}$ were approximately 0.05 °C and 0.6 °C, respectively (inferred from the data plot), for a heating duration of 20 s. In this study, the VHCs at 33 $W \cdot cm^{-2}$ and 128 $W \cdot cm^{-2}$ were 0.22 °C and 0.53 °C for a heating duration of 2 min. The larger variation at lower intensity may be attributed to the influence of noise in the measurement when choosing the temperature at 0.5 s after the switch-on transition in the "wait then measure" method.

TABLE VI. The average VHCs obtained from three repeat heating measurements for all transducer drive conditions obtained in this study. The standard deviations in the uncorrected and corrected peak temperatures were calculated and added together in quadrature to estimate the UC. VHC [%] is the fractional correction related to the uncorrected peak temperature.

On-time (mins)	Power (W)	Intensity ($W \cdot cm^{-2}$)	VHC (°C)	UC (%)	VHC% (%)
2	1.1	33	0.22	1.5	4.8
2	2.2	65	0.42	1.5	4.7
2	3.3	98	0.47	2.3	3.6
2	4.3	128	0.53	1.0	3.1
3	1.1	33	0.14	1.1	2.8
3	2.2	65	0.31	1.4	3.1
3	3.3	98	0.80	3.0	5.5
4	1.1	33	0.14	0.9	2.6
4	2.2	65	0.40	1.6	3.9
4	3.3	98	0.73	2.2	4.7

F. Comparison of the measured and predicted peak temperature rises

The peak temperature rises (actual temperatures–background temperature) of TC0 obtained from the measurements and simulations are listed in Table VII along with expanded uncertainties ($k = 2$). VHCs were applied to the measured temperature-time recordings and then the peak temperature rises were estimated. The measurement and simulation results show an agreement, i.e., their respective uncertainty intervals defined by the expanded uncertainties overlap. The worst-case difference in simulated temperatures across all heating conditions with respect to measurements was 6.7% at 98 $W \cdot cm^{-2}$ for 3 min heating. The measured peak temperature rises show higher differences in the simulations except at 1.1 W for heating durations of 2 and 3 min, the possible reasons for which are stated in Sec. VI.

VI. SUMMARY AND DISCUSSION

In this study, measurement-based simulation of temperature rises from focused ultrasound fields in the linear acoustic regime using k-Wave was investigated for its accuracy against experiments. The experiments involved a TTP made of agar-based TMM and included four fine wire TCs. A focused ultrasound transducer (1.06 MHz) aligned at the central thermocouple, TC0 to produce different acoustic powers (from 1.1 to 4.3 W) under CW excitation was used. The temperature rise experiments were conducted for different durations (from 2 to 4 min).

The acoustic wave propagation and heat diffusion were modelled using the k-Wave simulation toolkit and experimentally derived transducer source conditions. For an accurate representation of the curved transducer in the acoustic model, the output of the transducer was measured using a hydrophone over a plane perpendicular to the beam axis, and a planar equivalent source term was calculated. A 3D acoustic simulation was completed in water and tissue mimicking material layered media with an equivalent source positioned in water. The pressure field within the tissue

TABLE VII. The measured and predicted peak temperature rises at TC0. The parenthetical values are expanded uncertainties stated at a coverage probability of approximately 95% ($k = 2$).

On-time (mins)	Power (W)	Intensity ($W \cdot cm^{-2}$)	Measurement (°C)	Simulation (°C)	Difference w.r.t. Measurement (%)
2	1.1	33	4.4 (0.6)	4.6 (1)	4.5
2	2.2	65	8.5 (1)	8.9 (2)	4.7
2	3.3	98	12.7 (1.2)	13.2 (3)	3.9
2	4.3	128	16.4 (1.3)	17.5 (4)	6.7
3	1.1	33	5.0 (0.6)	5.0 (1.1)	0.0[a]
3	2.2	65	9.6 (1.1)	9.7 (2.2)	1.0
3	3.3	98	13.6 (1.5)	14.4 (3.2)	5.9
4	1.1	33	5.4 (0.7)	5.3 (1.2)	−1.9
4	2.2	65	9.9 (1.1)	10.3 (2.4)	4.0
4	3.3	98	14.7 (1.5)	15.2 (3.5)	3.4

[a]A difference of 0.0% arises due to rounding the results to one decimal place.

mimicking region was used to compute the heat source to simulate heating of the material. Temperature rises corresponding to the locations of four thermocouples in the thermal test phantom were recorded for comparison with the measurements.

Uncertainty analysis was performed for both the experimental setup and simulation model. For the experiments, various factors such as thermocouple accuracy, viscous heating effects, and uncertainty in acoustic power measurements were considered. Viscous heating corrections for the thermocouple were applied to the experimental data using the "wait then measure" method. For the simulation model, various factors such as the errors in equivalent source reconstruction, acoustic simulation grid convergence, and uncertainty in measured input parameters of the thermal model were considered.

A few aspects that were not considered in this study in explaining the differences between measurements and simulations are discussed here. First, the placement or positions of TCs within the TTP were not known exactly, but it relied upon the geometrical accuracy of the 3D-printed cylindrical holder. However, it is entirely feasible that the TCs would be slightly displaced during the pouring of the molten TMM during fabrication. Nevertheless, TC0 was always aligned to the acoustic focus, and its position uncertainty was mainly in the axial direction, whereas other TCs have position uncertainties both in axial and lateral directions. Therefore, there is greater confidence in the quantitative comparison of temperature-time data of TC0 from measurements and simulations, but the comparison is more of a qualitative nature for other TCs. Second, the simulations were performed at a constant temperature and did not consider the temperature dependence of TMM properties, i.e., the acoustic and thermal simulations were not coupled. The sound-speed[65] of IEC TMM has been found to increase with temperature at a rate of $1.5\,m \cdot s^{-1} \cdot ^{\circ}C^{-1}$ from 19.8 to 45.3 °C, whereas the acoustic attenuation has been found to decrease with temperature in two studies[66,67] at a rate of $0.005\,dB \cdot cm^{-1} \cdot MHz^{-1} \cdot ^{\circ}C^{-1}$ from 22 to 37 °C. Between the two coefficients, the proportional effect of attenuation is higher compared to the sound-speed change with temperature. However, the decreasing attenuation with temperature, which is not considered in the acoustic and thermal model, may have partly contributed to the differences between the simulations and measurements. Third, the transducer was characterised for its reference power levels on RFB using CW excitation, and the planar scanning of the transducer field for source reconstruction was performed using a 30-cycle tone burst. In a previous study,[22] acoustic powers measured in pulsed mode at different pulse repetition rates were not similar to CW when scaled by their duty factors that used RFB on two focused transducers from two distinct manufacturers.

Finally, it is worth mentioning that the IEC Technical Specification (TS) 62556:2014[68] provides guidelines on measurement and uncertainty evaluation of HITU fields to demonstrate compliance against IEC International Standard (IS) 60601-2–62:2013,[18] which applies to the basic safety and essential performance of high-intensity therapeutic ultrasound equipment. Moreover, the TS is restricted to linear propagation models, neglecting absorption. The IEC TS 63587 titled "Ultrasonics —Field characterization—Measurement-based simulation in water and other media" is currently at the draft stage, which includes areas such as model-based source reconstruction, requirements for hydrophone scanning, calibration of source levels such as acoustic power, and estimation of simulation uncertainties. Also, the scope of draft IEC TS 63587 does not stipulate accuracy metrics for simulated quantities or any particular field quantities as simulation outputs, and no such attempt was made within this article. The simulation output quantities were resolved to agree with measurements, having considered a detailed assessment of uncertainties, and that the uncertainties of measurement and simulation overlapped. The difference in simulated temperature rises across all heating conditions with respect to measurements ranged from −1.9% to 6.7%.

SUPPLEMENTARY MATERIAL

See the supplementary material for further details on experiments, results, and computational resources used for simulations.

ACKNOWLEDGMENTS

This work was supported in part by the European Metrology Programme for Innovation and Research (EMPIR) in the framework of the European Association of National Metrology Institutes (EURAMET), co-financed by the Participating States, through the 18HLT06 RaCHy Project under Grant No. 10.13039/100014132, the European Union's Horizon 2020 Research and Innovation Program and the Department for Science, Innovation and Technology through UK National Measurement System. Nicole Anstey and Aoife Ivory are thanked for their contribution to acoustic power measurements.

AUTHOR DECLARATIONS

Conflict of Interest

The authors have no conflicts to disclose.

DATA AVAILABILITY

The data used in the plots are openly available at https://zenodo.org/uploads/15384247. The k-Wave simulation codes developed for this study are available from https://gitlab.npl.co.uk/uua-public/k-wave-diffusion-accuracy. The data that support the findings of this study are available from the corresponding author upon reasonable request, with a turnaround period of eight weeks.

[1]W. D. O'Brien, "Ultrasound-biophysics mechanisms," Prog. Biophys. Mol. Biol. **93**, 212–255 (2007).

[2]B. J. Fowlkes, "American Institute of Ultrasound in Medicine consensus report on potential bioeffects of diagnostic ultrasound," J. Ultrasound Med. **27**, 503–515 (2008).

[3]A. J. Swerdlow, *Health Effects of Exposure to Ultrasound and Infrasound* (HPA, London, UK, 2010).

[4]K. B. Bader, F. Padilla, K. J. Haworth, N. Ellens, D. Dalecki, D. L. Miller, and K. A. Wear, "Overview of therapeutic ultrasound applications and safety considerations: 2024 update," J. Ultrasound Med. **44**, 381–634 (2025).

[5]D. Miller, N. Smith, M. Bailey, G. Czarnota, K. Hynynen, I. Makin, and Ultrasound in Medicine Bioeffects Committee, "Overview of therapeutic ultrasound applications and safety considerations," J. Ultrasound Med. **31**, 623–634 (2012).

[6]N. Okada, M. Shiiba, S. Takeuchi, T. Uchida, M. Yoshioka, and M. K. Kurosawa, "Durability test and observation on non-linear distortion in output waveform of anti-cavitation hydrophone in high intensity ultrasound," in *Proceedings of the 2014 IEEE International Ultrasonics Symposium* (2014), pp. 1551–1554.

[7]G. Xing, V. Wilkens, and P. Yang, "Review of field characterization techniques for high intensity therapeutic ultrasound," Metrologia **58**, 022001 (2021).

[8]C. R. Bawiec, T. D. Khokhlova, O. A. Sapozhnikov, P. B. Rosnitskiy, B. W. Cunitz, M. A. Ghanem, C. Hunter, W. Kreider, G. R. Schade, P. V. Yuldashev, and V. A. Khokhlova, "A prototype therapy system for boiling histotripsy in abdominal targets based on a 256-element spiral array," IEEE Trans. Ultrason, Ferroelect, Freq. Contr. **68**, 1496–1510 (2021).

[9]IEC 60601-2-37:2007+AMD1:2015 CSV: *Medical Electrical Equipment—Part 2-37: Particular Requirements for the Basic Safety and Essential Performance of Ultrasonic Medicaldiagnostic and Monitoring Equipment* (International Electrotechnical Commission, Geneva, Switzerland, 2015).

[10]K. Wear, *Marketing Clearance of Diagnostic Ultrasound Systems and Transducers - Guidance for Industry and Food and Drug Administration Staff* (U.S. Food and Drug Administration, Silver Spring, MD, 2023), https://www.fda.gov/regulatory-information/search-fda-guidance-documents/marketing-clearance-diagnostic-ultrasound-systems-and-transducers.

[11]IEC 62359:2011+A1:2018: *Ultrasonics – Field Characterization – Test Methods for the Determination of Thermal and Mechanical Indices Related to Medical Diagnostic Ultrasonic Fields (IEC 62359:2010)* (International Electrotechnical Commission, Geneva, Switzerland, 2018).

[12]"AIUM Official Statement for the Statement on Biological Effects of Therapeutic Ultrasound," J. Ultrasound Med. **42**(12), E68–E73 (2023).

[13]IEC 62127-3:2022: *Ultrasonics—Hydrophones—Part 3: Properties of Hydrophones for Ultrasonic Fields* (International Electrotechnical Commission, Geneva, Switzerland, 2022).

[14]IEC 61161:2013: *Ultrasonics—Power Measurement—Radiation Force Balances and Performance Requirements* (International Electrotechnical Commission, Geneva, Switzerland, 2013).

[15]IEC 62555:2013: *Ultrasonics—Power Measurement—High Intensity Therapeutic Ultrasound (HITU) Transducers and Systems* (International Electrotechnical Commission, Geneva, Switzerland, 2013).

[16]K. Beissner, "Radiation force and force balances," in *Ultrasonic Exposimetry*, edited by P. A. Lewin and M. C. Ziskin (CRC Press, Boca Raton, FL, 1992), pp. 163–168.

[17]IEC 60601-2-5:2015: *Medical Electrical Equipment Part 2-5: Particular Requirements for the Basic Safety and Essential Performance of Ultrasonic Physiotherapy Equipment* (International Electrotechnical Commission, Geneva, Switzerland, 2015).

[18]IEC 60601-2-62:2013: *Medical Electrical Equipment—Part 2-62: Particular Requirements for the Basic Safety and Essential Performance of High Intensity Therapeutic Ultrasound (HITU) Equipment* (International Electrotechnical Commission, Geneva, Switzerland, 2015).

[19]C. Koch and K.-V. Jenderka, "Final report on key comparison CCAUV. U-K3 for ultrasonic power," Metrologia **51**, 09001 (2014).

[20]S. Rajagopal, C. R. Fury, B. Zeqiri, M. Brandt, V. Wilkens, C. Koch, Y. Matsuda, M. Yoshioka, Y. Ping, Z. Yan, B. Wenping, R. P. B. Costa Felix, and E. G. Oliveira, "Report on BIPM/CIPM key comparison CCAUV.U-K4: Absolute calibration of medical hydrophones in the frequency range 0.5 MHz to 20 MHz," Metrologia **53**, 09004 (2016).

[21]G. R. Harris, S. M. Howard, A. M. Hurrell, P. A. Lewin, M. E. Schafer, K. A. Wear, V. Wilkens, and B. Zeqiri, "Hydrophone measurements for biomedical ultrasound applications: A review," IEEE Trans. Ultrason. Ferroelectr. Freq. Control **70**, 85–100 (2023).

[22]S. Maruvada, G. R. Harris, B. A. Herman, and R. L. King, "Acoustic power calibration of high-intensity focused ultrasound transducers using a radiation force technique," J. Acoust. Soc. Am. **121**, 1434–1439 (2007).

[23]S. Rajagopal and A. Shaw, "Erratum: The buoyancy method—A potential new primary ultrasound power standard," Metrologia **49**, 411 (2012).

[24]S. Maruvada, Y. Liu, J. E. Soneson, B. A. Herman, and G. R. Harris, "Comparison between experimental and computational methods for the acoustic and thermal characterization of therapeutic ultrasound fields," J. Acoust. Soc. Am. **137**, 1704–1713 (2015).

[25]O. V. Bessonova and V. Wilkens, "Membrane hydrophone measurement and numerical simulation of HIFU fields up to developed shock regimes," IEEE Trans. Ultrason. Ferroelectr. Freq. Control **60**, 290–300 (2013).

[26]O. A. Sapozhnikov, S. A. Tsysar, V. A. Khokhlova, and W. Kreider, "Acoustic holography as a metrological tool for characterizing medical ultrasound sources and fields," J. Acoust. Soc. Am. **138**, 1515–1532 (2015).

[27]V. A. Khokhlova, P. V. Yuldashev, P. B. Rosnitskiy, A. D. Maxwell, W. Kreider, M. R. Bailey, and O. A. Sapozhnikov, "Design of HIFU transducers to generate specific nonlinear ultrasound fields," in *Physics Procedia* (Elsevier, Amsterdam, the Netherlands, 2016), pp 132–138.

[28]B. E. Treeby and B. T. Cox, "k-Wave: MATLAB toolbox for the simulation and reconstruction of photoacoustic wave fields," J. Biomed. Opt. **15**, 021314 (2010).

[29]B. E. Treeby, J. Jaros, A. P. Rendell, and B. T. Cox, "Modeling nonlinear ultrasound propagation in heterogeneous media with power law absorption using a k-space pseudospectral method," J. Acoust. Soc. Am. **131**, 4324–4336 (2012).

[30]B. E. Treeby and B. T. Cox, "Modeling power law absorption and dispersion for acoustic propagation using the fractional Laplacian," J. Acoust. Soc. Am. **127**, 2741–2748 (2010).

[31]J. Jaros, A. P. Rendell, and B. E. Treeby, "Full-wave nonlinear ultrasound simulation on distributed clusters with applications in high-intensity

focused ultrasound," Int. J. High Perform. Comput. Appl. **30**(2), 137–155 (2016).

[32]J.-F. Aubry, O. Bates, C. Boehm, K. Butts Pauly, D. Christensen, C. Cueto, P. Gélat, L. Guasch, J. Jaros, Y. Jing, R. Jones, N. Li, P. Marty, H. Montanaro, E. Neufeld, S. Pichard, G. Pinton, A. Pulkkinen, A. Stanziola, A. Thielscher, B. Treeby, and E. van 't Wout, "Benchmark problems for transcranial ultrasound simulation: Intercomparison of compressional wave models," J. Acoust. Soc. Am. **152**, 1003–1019 (2022).

[33]B. T. Cox, J. G. Laufer, K. P. Kostli, and P. C. Beard, "Experimental validation of photoacoustic k-space propagation models," in *Photons Plus Ultrasound: Imaging and Sensing*, edited by A. A. Oraevsky and L. V. Wang (SPIE, Philadelphia, PA, 2004), pp. 238–248.

[34]K. Wang, E. Teoh, J. Jaros, and B. E. Treeby, "Modelling nonlinear ultrasound propagation in absorbing media using the k-Wave toolbox: Experimental validation," in *2012 IEEE International Ultrasonics Symposium*, Dresden, Germany (October 17-10, 2012) (IEEE, New York, 2013).

[35]E. Martin and B. E. Treeby, "Experimental validation of computational models for large-scale nonlinear ultrasound simulations in heterogeneous, absorbing fluid media," AIP Conf. Proc. **1685**, 070007 (2015).

[36]J. Robertson, E. Martin, B. Cox, and B. E. Treeby, "Sensitivity of simulated transcranial ultrasound fields to acoustic medium property maps," Phys. Med. Biol. **62**, 2559–2580 (2017).

[37]E. Martin, J. Jaros, and B. E. Treeby, "Experimental validation of k-Wave: Nonlinear wave propagation in layered, absorbing fluid media," IEEE Trans. Ultrason. Ferroelectr. Freq. Control **67**, 81–91 (2020).

[38]C. Constans, P. Mateo, M. Tanter, and J. F. Aubry, "Potential impact of thermal effects during ultrasonic neurostimulation: Retrospective numerical estimation of temperature elevation in seven rodent setups," Phys. Med. Biol. **63**(2), 025003 (2018).

[39]M. Hansen, D. Christensen, and A. Payne, "Experimental validation of acoustic and thermal modeling in heterogeneous phantoms using the hybrid angular spectrum method," Int. J. Hyperthermia **38**, 1617–1626 (2021).

[40]R. Xu, B. E. Treeby, and E. Martin, "Experiments and simulations demonstrating the rapid ultrasonic rewarming of frozen tissue cryovials," J. Acoust. Soc. Am. **153**, 517–528 (2023).

[41]P. Miloro, E. Martin, and A. Shaw, "Temperature elevation measured in a tissue-mimicking phantom for transvaginal ultrasound at clinical settings," Ultrasound **25**, 6–15 (2017).

[42]S. Rajagopal, N. Sadhoo, and B. Zeqiri, "Reference characterisation of sound speed and attenuation of the IEC agar-based tissue-mimicking material up to a frequency of 60 MHz," Ultrasound Med. Biol. **41**, 317–333 (2015).

[43]R. M. Baêsso, R. P. B. Costa-Felix, P. Miloro, and B. Zeqiri, "Ultrasonic parameter measurement as a means of assessing the quality of biodiesel production," Fuel **241**, 155–163 (2019).

[44]J. M. M. Pinkerton, "The absorption of ultrasonic waves in liquids and its relation to molecular constitution," Proc. Phys. Soc. B **62**, 129–141 (1949).

[45]M. O'Donnell, E. T. Jaynes, and J. G. Miller, "Kramers–Kronig relationship between ultrasonic attenuation and phase velocity," J. Acoust. Soc. Am. **69**, 696–701 (1981).

[46]K. V. Jenderka, G. Durando, B. Karaböce, S. Rajagopal, and A. Shaw, "Inter-laboratory comparison of HITU power measurement methods and capabilities," J. Phys. Conf. Series **279** 012015 (2011).

[47]IEC 61828:2020: *Ultrasonics—Transducers—Definitions and Measurement Methods regarding Focusing for the Transmitted Fields* (International Electrotechnical Commission, Geneva, Switzerland, 2020).

[48]E. Martin, Y. T. Ling, and B. E. Treeby, "Simulating focused ultrasound transducers using discrete sources on regular Cartesian grids," IEEE Trans. Ultrason. Ferroelecrtr. Freq. Control **63**, 1535–1542 (2016).

[49]B. Treeby, F. Lucka, E. Martin, and B. T. Cox, "Equivalent-source acoustic holography for projecting measured ultrasound fields through complex media," IEEE Trans. Ultrason. Ferroelectr. Freq. Control **65**, 1857–1864 (2018).

[50]K. A. Wear and A. Shah, "Nominal versus actual spatial resolution: Comparison of directivity and frequency-dependent effective sensitive element size for membrane, needle, capsule, and fiber-optic hydrophones," IEEE Trans. Ultrason, Ferroelect, Freq. Contr. **70**, 112–119 (2023).

[51]IEC 62127-1:2022: *Ultrasonics—Hydrophones—Part 1: Measurement and Characterization of Medical Ultrasonic Fields* (International Electrotechnical Commission, Geneva, Switzerland, 2022).

[52]K. A. Wear, "Spatiotemporal deconvolution of hydrophone response for linear and nonlinear beams—Part I: Theory, spatial-averaging correction formulas, and criteria for sensitive element size," IEEE Trans. Ultrason. Ferroelectr. Freq. Control **69**, 1243–1256 (2022).

[53]K. A. Wear, A. Shah, and C. Baker, "Spatiotemporal deconvolution of hydrophone response for linear and nonlinear beams—Part II: Experimental validation," IEEE Trans. Ultrason. Ferroelectr. Freq. Control **69**, 1257–1267 (2022).

[54]BIPM, IEC, IFCC, ILAC, ISO, IUPAC, IUPAP, *Guide to the Expression of Uncertainty in Measurement—Part 1: Introduction* (Sevres, Paris, France, 2023).

[55]W. J. Fry and R. B. Fry, "Determination of absolute sound levels and acoustic absorption coefficients by thermocouple probes—Theory," J. Acoust. Soc. Am. **26**, 294–310 (1954).

[56]W. J. Fry and R. Baumann, "Determination of absolute sound levels and acoustic absorption coefficients by thermocouple probes—Experiment," J. Acoust. Soc. Am. **26**, 311–317 (1954).

[57]H. Morris, I. Rivens, A. Shaw, and G. Ter Haar, "Investigation of the viscous heating artefact arising from the use of thermocouples in a focused ultrasound field," Phys. Med. Biol. **53**, 4759–4776 (2008).

[58]T. Tiennot, H. A. S. Kamimura, S. A. Lee, C. Aurup, and E. E. Konofagou, "Numerical modeling of ultrasound heating for the correction of viscous heating artifacts in soft tissue temperature measurements," Appl. Phys. Lett. **114**, 203702 (2019).

[59]S. Ambrogio, R. M. Baêsso, F. Bosio, F. Fedele, K. V. Ramnarine, B. Zeqiri, and P. Miloro, "A standard test phantom for the performance assessment of magnetic resonance guided high intensity focused ultrasound (MRgHIFU) thermal therapy devices," Int. J. Hyperthermia **39**, 57–68 (2022).

[60]S. Maruvada, Y. Liu, W. F. Pritchard, B. A. Herman, and G. R. Harris, "Comparative study of temperature measurements in *ex vivo* swine muscle and a tissue-mimicking material during high intensity focused ultrasound exposures," Phys. Med. Biol. **57**, 1–19 (2012).

[61]H. Morris, "Temperature measurement in *ex-vivo* bovine liver using fine-wire and thin-film thermocouples," AIP Conf. Proc. **829**, 633–637 (2006).

[62]B. Zeqiri, A. Cook, L. Rétat, J. Civale, and G. Ter Haar, "On measurement of the acoustic nonlinearity parameter using the finite amplitude insertion substitution (FAIS) technique," Metrologia **52**, 406–422 (2015).

[63]IEC 62127-2:2025: *Ultrasonics—Hydrophones—Part 2: Calibration for Ultrasonic Fields* (International Electrotechnical Commission, Geneva, Switzerland, 2025).

[64]BIPM, IEC, IFCC, ILAC, ISO, IUPAC, IUPAP, and OIML, *Evaluation of Measurement Data—Supplement 1 to the "Guide to the Expression of Uncertainty in Measurement"— Propagation of Distributions Using a Monte Carlo Method* (Sèvres, Paris, France, 2008).

[65]R. Monteiro Souza, M. K. M. de Assis, R. Pereira Barretto da Costa-Félix, and A. Victor Alvarenga, "Speed of sound in the IEC tissue-mimicking material and its maintenance solution as a function of temperature," Ultrasonics **118**, 106564 (2022).

[66]M. P. Brewin, L. C. Pike, D. E. Rowland, and M. J. Birch, "The acoustic properties, centered on 20 MHZ, of an IEC agar-based tissue-mimicking material and its temperature, frequency and age dependence," Ultrasound Med. Biol. **34**, 1292–1306 (2008).

[67]J. E. Browne, K. V. Ramnarine, A. J. Watson, and P. R. Hoskins, "Assessment of the acoustic properties of common tissue-mimicking test phantoms," Ultrasound Med. Biol. **29**, 1053–1060 (2003).

[68]IEC TS 62556:2014: *Ultrasonics—Field Characterization—Specification and Measurement of Field Parameters for High Intensity Therapeutic Ultrasound (HITU) Transducers and Systems* (International Electrotechnical Commission, Geneva, Switzerland, 2014).